



**Michigan
Technological
University**

Michigan Technological University
Digital Commons @ Michigan Tech

Michigan Tech Publications

9-1-2016

Lengthscale effects on exchange coupling in Co-Pt L10 + L12 nanochessboards

Eric P. Vetter
University of Virginia

Liwei D. Geng
Michigan Technological University, liweig@mtu.edu

Priya Ghatwai
University of Virginia

Dustin A. Gilbert
NIST Center for Neutron Research

Yongmei M. Jin
Michigan Technological University, ymj@mtu.edu

See next page for additional authors

Follow this and additional works at: <https://digitalcommons.mtu.edu/michigantech-p>


 Part of the [Materials Science and Engineering Commons](#)

Recommended Citation

Vetter, E., Geng, L. D., Ghatwai, P., Gilbert, D., Jin, Y. M., Soffa, W., & Floro, J. (2016). Lengthscale effects on exchange coupling in Co-Pt L10 + L12 nanochessboards. *APL Materials*, 4(9). <http://doi.org/10.1063/1.4962187>

Retrieved from: <https://digitalcommons.mtu.edu/michigantech-p/2396>

Follow this and additional works at: <https://digitalcommons.mtu.edu/michigantech-p>

 Part of the [Materials Science and Engineering Commons](#)


Authors

Eric P. Vetter, Liwei D. Geng, Priya Ghatwai, Dustin A. Gilbert, Yongmei M. Jin, William A. Soffa, and Jerrold A. Floro

Lengthscale effects on exchange coupling in Co-Pt $L1_0 + L1_2$ nanochessboards

Cite as: APL Mater. 4, 096103 (2016); <https://doi.org/10.1063/1.4962187>

Submitted: 21 June 2016 . Accepted: 22 August 2016 . Published Online: 01 September 2016

Eric P. Vetter, Liwei Geng, Priya Ghatwai, Dustin A. Gilbert , Yongmei Jin, William A. Soffa, and Jerrold A. Floro



View Online



Export Citation



CrossMark

ARTICLES YOU MAY BE INTERESTED IN

[Exchange coupling effects in Co-Pt nanochessboards](#)

Journal of Applied Physics **123**, 093901 (2018); <https://doi.org/10.1063/1.5019841>


[What does a first-order reversal curve diagram really mean? A study case: Array of ferromagnetic nanowires](#)

Journal of Applied Physics **113**, 043928 (2013); <https://doi.org/10.1063/1.4789613>

[Probing the \$A1\$ to \$L1_0\$ transformation in FeCuPt using the first order reversal curve method](#)

APL Materials **2**, 086106 (2014); <https://doi.org/10.1063/1.4894197>

additive manufacturing epitaxial crystal growth cerium oxide polishing powder silver nanoparticles sputtering targets



THE ADVANCED MATERIALS MANUFACTURER®

deposition slugs OLED Lighting spintronics solar energy

osmium nanoribbons thin films chalcogenides AuNPs

GDC li-ion battery electrolytes 99.999% ruthenium spheres

endohedral fullerenes copper nanoparticles diamond micropowder

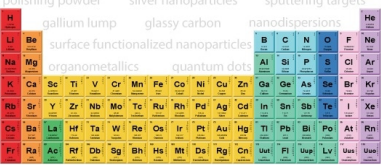
CIGS MBE grade materials palladium catalysts flexible electronics

beta-barium borate borosilicate glass dysprosium pellets YBCO

pyrolytic graphite 3d graphene foam indium tin oxide mesoporous silica

raman substrates sapphire windows tungsten carbide InGaAs

barium fluoride carbon nanotubes lithium niobate scandium powder



gallium lump glassy carbon nanodispersions

surface functionalized nanoparticles organometallics quantum dot

III-IV semiconductors CVD precursors europium phosphors

InAs wafers laser crystals ultra high purity materials MOFs

rare earth metals photovoltaics refractory metals MOCVD

superconductors transparent ceramics ultra high purity silicon

*American Elements opens up a world of possibilities so you can **Now Invent!***

Over 15,000 certified high purity laboratory chemicals, metals, & advanced materials and a state-of-the-art Research Center. Printable GHS-compliant Safety Data Sheets. Thousands of new products. And much more. All on a secure multi-language "Mobile Responsive" platform.

perovskite crystals yttrium iron garnet alternative energy h-BN

gold nanocubes graphene oxide macromolecules photonics

rhodium sponge fiber optics beamsplitters infrared dyes zeolites

fused quartz metallocenes platinum ink buckyballs Ti-6Al-4V

Now Invent.™
The Next Generation of Material Science Catalogs

www.americanelements.com

Lengthscale effects on exchange coupling in Co-Pt $L1_0 + L1_2$ nanochessboards

Eric P. Vetter,¹ Liwei Geng,² Priya Ghatwai,¹ Dustin A. Gilbert,³
Yongmei Jin,² William A. Soffa,¹ and Jerrold A. Floro^{1,a}

¹*Department of Materials Science and Engineering, University of Virginia, Charlottesville, Virginia 22903, USA*

²*Department of Materials Science and Engineering, Michigan Technological University, Houghton, Michigan 49931, USA*

³*NIST Center for Neutron Research, National Institute of Standards and Technology, Gaithersburg, Maryland 20899, USA*

(Received 21 June 2016; accepted 22 August 2016; published online 1 September 2016)

The Co-Pt nanochessboard is a quasi-periodic, nanocomposite tiling of $L1_0$ and $L1_2$ magnetic phases that offers a novel structure for the investigation of exchange coupling, relevant to permanent magnet applications. Periodicity of the tiling is controlled by the rate of cooling through the eutectoid isotherm, resulting in control over the $L1_0$ - $L1_2$ exchange coupling. First order reversal curve analysis reveals a transition from partial coupling to nearly complete exchange-coupling in a $\text{Co}_{40.2}\text{Pt}_{59.8}$ nanochessboard structured alloy as the periodicity is reduced below the critical correlation length. Micromagnetic simulations give insights into how exchange coupling manifests in the tiling, and its impact on microscopic magnetization reversal mechanisms. © 2016 Author(s). All article content, except where otherwise noted, is licensed under a Creative Commons Attribution (CC BY) license (<http://creativecommons.org/licenses/by/4.0/>). [<http://dx.doi.org/10.1063/1.4962187>]

Exchange coupled nanocomposite magnetic materials have been key in the development of magnetic recording and spintronic technologies,¹⁻⁴ but recently have been explored in the development of improved composite permanent magnets.^{5,6} In principle, exchange coupling a high-anisotropy magnetic material to a high-moment, magnetically soft material results in a nanocomposite that can exhibit an enhanced moment and a large coercivity.^{6,7} Ideally, these factors result in an improvement in the maximum energy product of the magnet. In thin films, exchange coupling can be directly controlled through choice of film materials,⁸ thicknesses, and interfaces.⁹ In bulk materials, exchange coupling is achieved through artificial compositing¹⁰ or processing methods¹¹ that create phase separation on the nanoscale.

A novel bulk nanocomposite was investigated by Leroux *et al.*, who showed that the eutectoid transformation, $A1 \rightarrow L1_0 + L1_2$, in the binary Co-Pt system¹² could result in a nanochessboard microstructure. This self-assembled 2 + 1-D structure consists of magnetically hard $L1_0$ (tetragonal) nanorods embedded in a soft $L1_2$ (cubic) matrix with fully coherent interfaces. When viewed down the rod axis, a characteristic chessboard pattern is revealed. This fascinating microstructure provides an excellent platform for studying exchange coupling at the nanoscale that is topologically intermediate between idealized 1-D coupling in thin films, and the more complex, inherently 3-D environment associated with bulk nanocomposite magnets.

Here we investigate the magnetic properties of fully transformed CoPt nanochessboards with tailored periodicity, achieved by controlling the cooling rate during thermal annealing of the samples. Increasing the periodicity decouples the hard and soft phases. Magnetic reversal behavior is investigated using the first order reversal curve (FORC) technique, which shows control of the magnetic exchange coupling associated with the microstructure. Micromagnetic

^aAuthor to whom correspondence should be addressed. Electronic mail: jaf9r@virginia.edu

simulations are performed to better understand magnetic behavior in this unusual nanocomposite.

A boule of $\text{Co}_{40.2}\text{Pt}_{59.8}$ was formed by arc-melting Co (99.9%) and Pt (99.99%). The resulting button consisted of a metastable, polycrystalline, A1 (FCC) solid solution of Co and Pt with 20-40 μm grain size, as discussed previously.^{13,14} To promote the phase transformation $\text{A1} \rightarrow \text{L1}_0 + \text{L1}$, encapsulated samples were slow-cooled through the eutectoid isotherm (nominally 736 °C)¹² at various rates and then held isothermally for several days prior to quenching. The two samples of interest here were cooled from 750 °C to 600 °C at a rate of 40 °C/day or 80 °C/day and then isothermally annealed at 600 °C for 1 week or 4 days, respectively. These will be referred to as the “40CPD” and “80CPD” samples. The microstructure of these samples was examined using transmission electron microscopy (TEM). X-ray diffraction analysis was also performed and supports the two-phase coexistence, but it is non-trivial to analyze due to large coherency effects and will be reported elsewhere.

Magnetic measurements were performed at room temperature using a vibrating sample magnetometer (VSM) with a sweep rate of 50 mT/s and an averaging time of 0.5 s. FORCs were obtained by starting at positive saturation and decreasing the magnetic field to a scheduled reversal field, H_r . Then, the magnetization is measured as the applied magnetic field, H , is increased from H_r to positive saturation, thus measuring a single reversal curve. A total of 144 reversal curves were measured for H_r between -1.8 T and 1.8 T with field steps of 25 mT, collecting a family of FORCs. The FORC distribution is calculated as a mixed second derivative of the magnetization with respect to H and H_r using the VARIFORC¹⁵ program within the FORCinel software package.¹⁶ It is convenient to plot the FORC distribution in a rotated coordinate system with axes H_c and H_u such that $H_c = (H - H_r)/2$ and $H_u = (H + H_r)/2$, where H_c and H_u represent coercive and interaction field distributions, respectively.¹⁷

TEM is the simplest means of confirming the presence of chessboard structure. TEM micrographs on a [001] zone axis using the (110) superlattice reflection for dark field (DF) imaging are shown in Fig. 1 for 40CPD and 80CPD samples. The [100] and [010] L1_0 easy-axis variants in the [001]-oriented chessboard (i.e., the long axis of the nanorods is oriented parallel to [001]) both appear dark against the bright background of the cubic L1_2 matrix. The 40CPD sample has characteristic tiling dimensions of about 25-40 nm, while in the 80CPD sample the lateral phase dimensions are about 10-20 nm. Figure 1 shows individual “colonies” of the eutectoid chessboard. Within each large parent grain of the original polycrystalline A1 material, numerous chessboard colonies form along all three $\langle 100 \rangle$ directions of the parent phase, with typical colony lengthscales of 100-500 nm.¹⁴ TEM surveys of multiple parent grains were performed to ensure the micrographs are representative. It will be important to recall, when interpreting the magnetic properties obtained by VSM, that macroscopically the sample is a randomly oriented bulk polycrystal.

The FORC distributions are shown in Fig. 2 along with the corresponding raw M-H FORC data for the 40CPD and 80CPD samples. In the raw FORCs, the outer envelope is identical with the conventional hysteresis loop. Comparison of the FORC diagrams shows stark differences. The FORC diagram from the 40CPD sample, Fig. 2(a), displays two peaks centered at $\mu_0 H_c = 0$ mT, $\mu_0 H_u = 40$ mT and $\mu_0 H_c = 247.5$ mT, $\mu_0 H_u = 0$ mT. These peaks indicate two-phase magnetic behavior,^{18,19} with the former identifying a soft magnetic phase, and the latter a hard phase. An additional low intensity lobe is seen extending from the soft phase diagonally out to approximately $\mu_0 H_c = 200$ mT, $\mu_0 H_u = -225$ mT which is coupled with an adjacent region of negative FORC density. This type of feature has been previously associated with magnetic interactions between hard and soft magnetic elements.²⁰ In contrast, the 80CPD sample, Fig. 2(c), displays only a single feature occurring at $\mu_0 H_c = 290$ mT, $\mu_0 H_u = -12$ mT with no diagonal lobe, identifying single-phase magnetic behavior.

For the 40CPD sample, the two clearly defined peaks observed in FORC distribution of Fig. 2(a) are connected by significant intensity, which indicates that *partial* exchange coupling is occurring. In comparison, the 80CPD sample, Fig. 2(c), shows only a single peak in the FORC density plot, centered at relatively large H_c . Since the TEM confirms that both L1_0 and L1_2 phases are present in this sample, the observed single-phase magnetic behavior in the presence of two ferromagnetic structural phases implies complete exchange coupling of the L1_2 phase to the harder

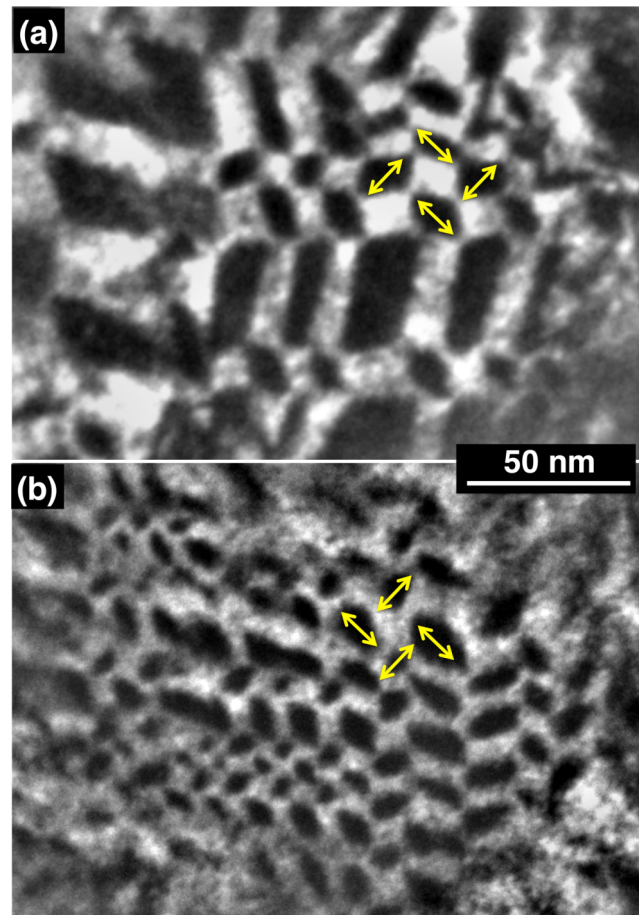


FIG. 1. (110) DF TEM imaged on the [001] zone axis for (a) 40CPD and (b) 80CPD samples. The arrows show the direction of the magnetic easy axis in the L_{10} nanorods.

L_{10} . The critical dimension below which complete exchange coupling is expected is approximated by $d_{cr} = 2\pi\sqrt{A_{soft}/2K_{hard}}$.⁷ Using the exchange stiffness $A = 2.5 \times 10^{-11}$ J/m and the magnetocrystalline anisotropy constant of the hard L_{10} phase,¹³ $K = 1.5 \times 10^6$ J/m³, we obtain $d_{cr} = 18$ nm. For the 80CPD sample, the transverse dimensions of the L_{12} regions (~ 10 -20 nm) are mostly below d_{cr} , consistent with nearly complete exchange coupling. As a result, it is expected that exchange coupling dominates the magnetic orientation within each columnar tile. However, for the 40CPD sample, the transverse size of a majority of the L_{12} tiles (~ 25 to 40 nm) exceeds d_{cr} , and hence a significant volume fraction of the soft phase is able to switch independent of the hard phase. This reduces the coercivity by allowing domain walls to form within the L_{12} regions, which promotes reversal at lower fields.^{21,22}

To qualitatively supplement and inform our interpretation of the observed magnetic behavior in nano-chessboards, extensive micromagnetic simulations were performed on idealized chessboard structures. The complete study will be published elsewhere; here we discuss select results relevant to the experimental data that better reveal the role of lengthscales in exchange coupling for this novel geometry, and identify potential reversal mechanisms. We emphasize that while these microscopic mechanisms should be valid, reversal in real chessboards is likely more complex owing to variability in tile sizes and shapes; also the lengthscale associated with the chessboard colony size is not yet included in the simulations, and may also play a key role in the domain magnetics.

Figure 3(a) shows the 2-D projected nano-chessboard configuration used in the simulations, with the black and white colors indicating the L_{10} and L_{12} phases, respectively. Since the L_{10} phase

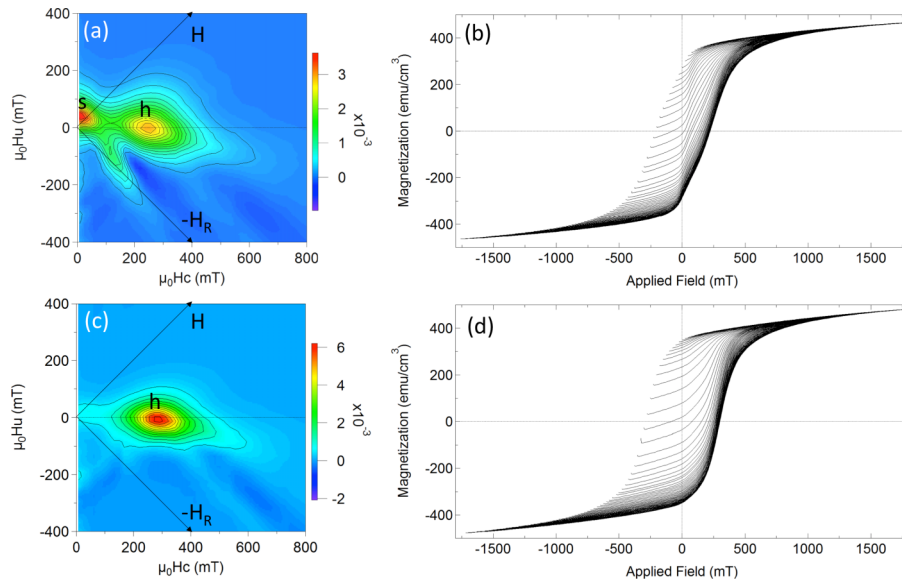


FIG. 2. FORC diagrams and corresponding raw M-H FORC data for 40CPD ((a) and (b)) and 80CPD ((c) and (d)) samples. In (a) and (c), the letters h and s identify the hard and soft peaks, respectively.

possesses uniaxial anisotropy, the corresponding $L1_0$ tiles in Fig. 3(a) have different easy axis directions depending on the crystalline orientation, which creates a complex local coupling environment. Furthermore, although we refer to the phase morphology as “tiles,” each tile is extended in the out-of-plane dimension, realizing a nanorod-like structure, which will not affect exchange coupling. The micromagnetic simulations are quasi-3-D—fields and moments have 3-D components, while the moments are assumed to be uniform along [001]. Periodic boundary conditions are enforced in the plane of the chessboard. The simulations consider two different sizes, $d = 12.6 \text{ nm} < d_{cr}$ and $d = 36 \text{ nm} > d_{cr}$, roughly representing the 80CPD and 40CPD samples, respectively. Magnetic field is applied along in-plane [100] and [110] and out-of-plane [001] directions. The simulated hysteresis curves and snapshots of typical domain structures are presented in Figs. 3(b)-3(g). Note that the simulations consider nanocheesboards of one crystallographic orientation while the real samples are polycrystalline with all orientation variants, thus no direct comparison should be made between the simulated and measured hysteresis curves. Additional descriptions of the methodology, and more domain snapshots, can be found in the [supplementary material](#).

Figure 3(b) shows the simulated hysteresis curves for the smaller lengthscale, $d = 12.6 \text{ nm} < d_{cr}$. In this case the nanocheesboard structure exhibits strong exchange coupling effects, which align the magnetizations of the $L1_0$ and $L1_2$ tiles, and *the two-phase material behaves effectively as a single-domain single-phase magnetic material*, as manifested in the hysteresis curves. The system exhibits an effective magnetic anisotropy with [110] easy axis and [001] hard axis, caused by the strong exchange coupling between adjacent $L1_0$ tiles via bridging by the $L1_2$ tiles. Domain structure in Figs. 3(d) and 3(e) corresponds to the points A1 and A2, respectively, in Fig. 3(b), where the former is near the saturation under [001] field while the latter is amid the magnetic reversal under in-plane [110] field. In both situations, nearly uniform magnetization occurs over the nanocheesboard, confirming complete exchange coupling, consistent with a single peak in the FORC density plot observed in the 80CPD sample.

In comparison, when the lengthscale is increased to $d = 36 \text{ nm} > d_{cr}$, exchange coupling is greatly reduced, the soft $L1_2$ tiles are unable to couple the hard $L1_0$ tiles, and the magnetizations of adjacent $L1_0$ tiles independently align along their individual easy axes. As a result, the nanocheesboard structure behaves as multi-domain two-phase material, manifested in the hysteresis curves shown in Fig. 3(c). The single-event reversal behavior by homogeneous rotation is replaced by heterogeneous magnetization in both phases. The multi-domain two-phase heterogeneous magnetization processes due to reduced exchange coupling explains the multi-step reversals in the

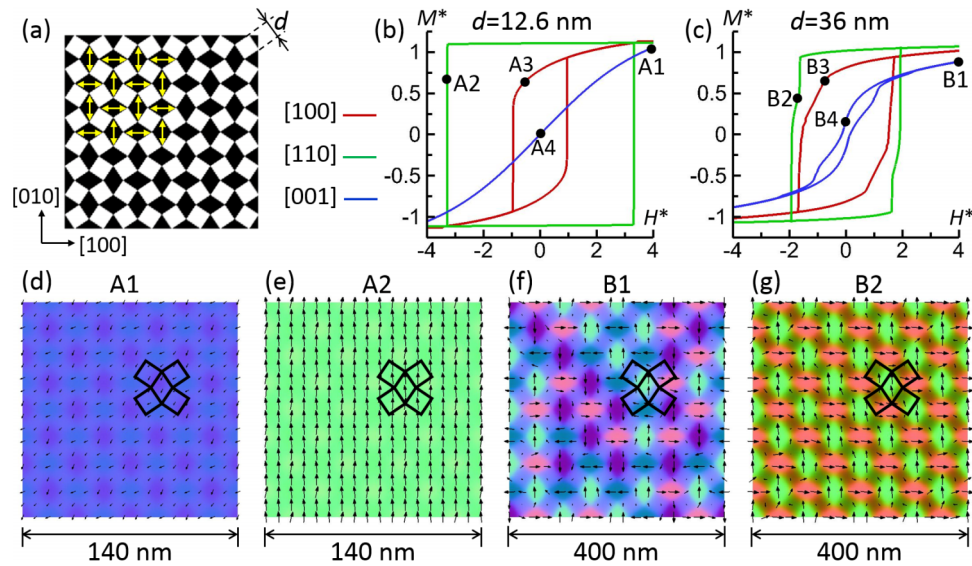


FIG. 3. (a) Micromagnetic simulation cell with L_{12} in white and L_{10} in black; yellow arrows label the easy axis in alternating L_{10} variants. Simulated hysteresis loops along three crystallographic directions for tile size $d = 12.6$ nm (b) and $d = 36.0$ nm (c). Magnetic field and magnetization are scaled with respect to the saturation magnetization of L_{10} phase. (d)–(g) Magnetic domain structures corresponding to A1, A2, B1, and B2 in the hysteresis loops in (b) and (c). The magnetization vector field is visualized by black arrows for in-plane components (m_x , m_y) and by color maps for its all three components (m_x , m_y , m_z), respectively in red, blue, and green values. The same group of four L_{12} tiles surrounding an L_{10} tile is highlighted in (d)–(g).

hysteresis curves in Fig. 3(c) and the two peaks in the FORC density plot observed in 40CPD sample.

The simulations also reveal an interesting domain phenomenon when $d = 36$ nm: the formation of out-of-plane magnetic domains in the soft L_{12} tiles and their important roles in magnetic reversal. *Perpendicular* domains form in some L_{12} tiles in the thermally demagnetized state (not shown here), under perpendicular $[001]$ field (exemplified in B1), and even under some in-plane fields (exemplified in B2). Perpendicular domains result from the shape anisotropy of the nanorods that dictates a $[001]$ easy axis in the L_{12} phase, which become significant only when the exchange coupling effects are weakened. Hence the magnetic reversal for $H \parallel [001]$ becomes hysteretic as shown in Fig. 3(c). Importantly, magnetic reversals under in-plane fields are facilitated by the perpendicular domains in the L_{12} tile, see the domain structure at B2 in Fig. 3(g). Whether a perpendicular domain in a particular L_{12} tile is formed depends on the adjacent L_{10} tiles. Among 16 possible magnetization configurations in the four adjacent L_{10} tiles, four configurations prefer a perpendicular domain in the enclosed L_{12} tile, which will be discussed in detail elsewhere. A perpendicular domain builds up magnetic charges at the interface between the L_{12} tile and its L_{10} neighbors, which generates magnetostatic interactions between adjacent L_{10} tiles. Long-range magnetostatic interactions between L_{12} regions could cause the observed soft phase peak in the FORC diagram to shift to positive H_u in Fig. 2(a).²³

The diagonal feature extending between the two phases in Fig. 2(a) is often referred to as an “interference” region.^{24,25} The interference region is aligned in H_r with the hard feature, and in H with the soft feature, suggesting that the down-switching (switching under an applied reversal field) of the hard layer produces new reversal events associated with the soft phase. Neighboring the interference feature is an associated negative feature; negative features have been demonstrated to result when up-switching events (re-reversal under an applied forward field in a FORC) shift in H due to a field-dependent interaction.²³ Thus the re-reversal of the hard phase manifests a shift in the up-switching field in the soft phase, realized through their exchange coupling. This is consistent with recent works that suggest a correlation between the interference region, the H_u shift of the soft phase feature, and the relative strength of the hard and soft phases.²⁵

In summary, bulk nanocomposite CoPt permanent magnets were synthesized based on the nanochessboard structure, with tunable hard-soft exchange coupling. Increasing the cooling rate during thermal processing of initially disordered Al Co_{40.2}Pt_{59.8} alloys resulted in a reduction of the periodicity of the resulting L₁₀ + L₁₂ nanochessboard microstructure. Concomitant increases in the degree of exchange coupling and permanent magnetic properties were seen in the major hysteresis loops and FORC diagrams. Micromagnetic simulations of idealized nanochessboards suggest explanations for key features in the FORC diagrams related to the degree of exchange coupling, and suggest reversal mechanisms deserving further study.

See [supplementary material](#) for a table of relevant permanent magnetic properties, FORC smoothing parameters, and for detailed experimental values and more information on the micromagnetic simulations and their results.

Funding from the NSF under Grant Nos. DMR-1105336 (P.G., E.P.V., W.A.S., and J.A.F.) and DMR-1409317 (L.G. and Y.J.) is gratefully acknowledged. Thanks to Richard Harrison for help with FORCinel and VARIFORC, and Christine Leroux for useful discussion. The parallel computer simulations were performed on XSEDE supercomputers.

- ¹ R. H. Victora and X. Shen, *IEEE Trans. Magn.* **41**, 537 (2005).
- ² D. Suess, T. Schrefl, S. Fahler, M. Kirschner, G. Hrkac, F. Dorfbauer, and J. Fidler, *Appl. Phys. Lett.* **87**, 012504 (2005).
- ³ S. Parkin, X. Jiang, C. Kaiser, A. Panchula, K. Roche, and M. Samant, *Proc. IEEE* **91**, 661 (2003).
- ⁴ H. Zeng, J. Li, J. P. Liu, Z. L. Wang, and S. Sun, *Nature* **420**, 395 (2002).
- ⁵ E. E. Fullerton, J. S. Jiang, and S. D. Bader, *J. Magn. Magn. Mater.* **200**, 392 (1999).
- ⁶ R. Skomski and J. M. D. Coey, *Phys. Rev. B* **48**, 15812 (1993).
- ⁷ E. F. Kneller and R. Hawig, *IEEE Trans. Magn.* **27**, 3560 (1991).
- ⁸ J. E. Davies, O. Hellwig, E. E. Fullerton, J. S. Jiang, S. D. Bader, G. T. Zimanyi, and K. Liu, *Appl. Phys. Lett.* **86**, 262503 (2005).
- ⁹ D. A. Gilbert, J. Olamit, R. K. Dumas, B. J. Kirby, A. J. Grutter, B. B. Maranville, E. Arenholz, J. A. Borchers, and K. Liu, *Nat. Commun.* **7**, 11050 (2016).
- ¹⁰ C. Rong, Y. Zhang, N. Poudyal, X. Xiong, M. J. Kramer, and J. Ping Liu, *Appl. Phys. Lett.* **96**(10), 102513 (2010).
- ¹¹ G. Hadjipanayis, *J. Magn. Magn. Mater.* **200**, 373 (1999).
- ¹² C. Leroux, A. Loiseau, D. Broddin, and G. Vantendeloo, *Philos. Mag. B* **64**, 57 (1991).
- ¹³ P. Ghatwai, E. Vetter, M. Hrdy, W. A. Soffa, and J. A. Floro, *J. Magn. Magn. Mater.* **375**, 87 (2015).
- ¹⁴ E. P. Vetter, P. Ghatwai, W. A. Soffa, and J. A. Floro, *IEEE Magn. Lett.* **6**, 6600104 (2015).
- ¹⁵ R. Egli, *Global Planet. Change* **110**, 302 (2013).
- ¹⁶ R. J. Harrison and J. M. Feinberg, *Geochem., Geophys., Geosyst.* **9**, Q05016, doi:10.1029/2008GC001987 (2008).
- ¹⁷ C. R. Pike, A. P. Roberts, and K. L. Verosub, *J. Appl. Phys.* **85**, 6660 (1999).
- ¹⁸ A. P. Roberts, C. R. Pike, and K. L. Verosub, *J. Geophys. Res.: Solid Earth* **105**, 28461, doi:10.1029/2000JB900326 (2000).
- ¹⁹ D. A. Gilbert, J.-W. Liao, L.-W. Wang, J. W. Lau, T. J. Klemmer, J.-U. Thiele, C.-H. Lai, and K. Liu, *APL Mater.* **2**, 086106 (2014).
- ²⁰ H. Chiriac, N. Lupu, L. Stoleriu, P. Postolache, and A. Stancu, *J. Magn. Magn. Mater.* **316**, 177 (2007).
- ²¹ X. M. Kou, X. Fan, R. K. Dumas, Q. Lu, Y. P. Zhang, H. Zhu, X. K. Zhang, K. Liu, and J. Q. Xiao, *Adv. Mater.* **23**, 1393 (2011).
- ²² D. Suess, J. Lee, J. Fidler, and T. Schrefl, *J. Magn. Magn. Mater.* **321**(6), 545 (2009).
- ²³ D. A. Gilbert, G. T. Zimanyi, R. K. Dumas, M. Winklhofer, A. Gomez, N. Eibagi, J. L. Vicent, and K. Liu, *Sci. Rep.* **4**, 4204 (2014).
- ²⁴ I. Panagiotopoulos, *J. Magn. Magn. Mater.* **323**, 2148 (2011).
- ²⁵ E. Jafari-Khamse, M. A. Kashi, and A. Ramazani, *Curr. Appl. Phys.* **16**, 486 (2015).